Establishment of rules for interpreting ultraviolet autofluorescence microscopy images for noninvasive detection of Barrett's esophagus and dysplasia

Bevin Lin
Shiro Urayama
Ramez M. G Saroufeem
Dennis L. Matthews
Stavros G. Demos

Establishment of rules for interpreting ultraviolet autofluorescence microscopy images for noninvasive detection of Barrett's esophagus and dysplasia

Bevin Lin,[a,b] **Shiro Urayama,**[c] **Ramez M. G Saroufeem,**[d] **Dennis L. Matthews,**[a,b] **and Stavros G. Demos**[a,e]
[a]University of California, Davis, NSF Center for Biophotonics Science and Technology, 4800 2nd Avenue, Sacramento, California 95817
[b]University of California, Davis, Department of Biomedical Engineering, One Shields Avenue, Davis, California 95616
[c]University of California, Davis Medical Center, Division of Gastroenterology and Hepatology, 4150 V Street, Suite 3500, Sacramento, California 95817
[d]University of California, Davis Medical Center, Department of Pathology, 4400 V Street, Sacramento, California 95817
[e]Lawrence Livermore National Laboratory, 7000 East Avenue, Livermore, California 94550

Abstract. The diagnostic potential of autofluorescence (AF) microscopy under ultraviolet (UV) excitation is explored using *ex vivo* human specimens. The aim is to establish optical patterns (the rules for interpretation) that correspond to normal and abnormal histologies of the esophagus, spanning from early benign modifications (Barrett's esophagus) to subsequent dysplastic change and progression toward carcinoma. This was achieved by developing an image library categorized by disease progression. We considered morphological changes of disease as they are compared with histological diagnosis of the pathological specimen, as well as control samples of normal esophagus, proximal stomach, and small intestine tissue. Our experimental results indicate that UV AF microscopy could provide real-time histological information for visualizing changes in tissue microstructure that are currently undetectable using conventional endoscopic methods. © *2012 Society of Photo-Optical Instrumentation Engineers (SPIE).* [DOI: 10.1117/1.JBO.17.1.016013]

Keywords: autofluorescence; medical imaging; microscopy; ultraviolet.

Paper 11367 received Jul. 12, 2011; revised manuscript received Nov. 1, 2011; accepted for publication Nov. 30, 2011; published online Feb. 13, 2012.

1 Introduction

Although the pathogenesis of esophageal adenocarcinoma (EAC) is still unclear,[1,2] there is a general consensus among the medical and research communities that the increasing rate of gastroesophageal reflux disease (GERD) has contributed to the annual increase of EAC incidence of more than 20% since 1975.[3,4] The associated mortality of EAC has increased more than seven times during this period, faster than any other malignancy in the United States.[5] GERD affects at least 15% to 20% of the adult population every week,[4,6] while 7% to 10% of the GERD population may suffer from chronic injury to the distal esophagus with a consequence of metaplastic changes in the distal esophageal lining,[3,4,7,8] a condition referred to as Barrett's esophagus (BE).

BE is considered a premalignant condition in which the stratified squamous epithelium of the distal esophagus is replaced with specialized intestinal epithelium (columnar epithelium containing goblet cells).[1,9] The current definition of BE requires both endoscopic documentation for the presence of glandular epithelial lining and the histological identification of specialized intestinal metaplasia with goblet cells in the esophagus,[10] the hallmark of BE.[1] Apart from repeated endoscopy and multiple biopsies, there is no definitive method of accurately evaluating which patients with BE will develop dysplasia (and ultimately carcinoma), although patients with long-segment, long-standing BE are more likely to demonstrate progression toward dysplasia/carcinoma. Recent studies suggest the gastroesophageal (GE) junction to be the site of metaplastic initiation, starting when the distal esophageal squamous mucosa is replaced by columnar epithelium similar to that seen in the gastric cardia.[9,11] This columnar mucosa of the distal esophagus has been histologically found to contain undetected BE in 15% to 24% of an endoscopically normal junction.[11] From a practical standpoint, this percentage may reflect the endoscopic appearance of the velvety-salmon texture-discoloration (suggestive of columnar-lined epithelium), which could be subjective and subtle. It should be noted, however, that the presence of intestinal metaplasia in the cardia (or any part of the stomach) is managed differently from BE patients.

The risk of BE patients developing cancer is divided into four histopathological categories: no dysplasia, indefinite for dysplasia, low-grade dysplasia (LGD), and high-grade dysplasia (HGD).[9,12] The histological pretreatment classification determines clinical management of the patient and often suffers from poor interobserver agreement.[13] For late-stage dysplastic lesions within the mucosa, local endoscopic management such as mucosal resection or ablation techniques have demonstrated efficacy without significant morbidity.[14–19] However, providing accurate histological diagnosis becomes critically important for identifying the clinical point at which to decide on early endoscopic intervention.

Address all correspondence to: Bevin Lin, University of California, Davis, Department of Biomedical Engineering, One Shields Avenue, Davis, California 95616. Tel: (916) 734-8600; E-mail: belin@ucdavis.edu

Dysplasia classification for pretreatment diagnosis is generally taken from the Vienna classification system[20,21] or has historically been transposed from criteria that define inflammatory bowel disease.[12,21] The histologic criterion used as reference in this work has been adopted from literature sources.[7,9,12,13] This compiled pathology diagnosis is defined in column 1 of Table 1; histological architecture and cytology are summarized in columns 2 and 3; and column 4 outlines the optical image morphology (the rules of interpretation) from which the work herein describes. These defining cellular features are essentially invisible to the endoscopist at the time of biopsy specimen collection. A positive biopsy sampling of dysplasia is thus commonly obtained randomly and subject to the previously mentioned inter- and intra-observer variability. These are two of the greatest challenges when providing optimal care to patients with BE.[12,13]

LGD, the earliest sign of malignant progression, has the least consistent agreement and lowest reproducibility among pathologists.[12,21,22] The standard option for physicians is to wait until HGD is identified during surveillance endoscopy procedures before electing for endoscopic or surgical treatment.[7] Research using confocal microscopy[23,24] has provided promising results toward real-time histology, generating the confocal Barrett's classification system.[25,26] This approach, however, requires application of contrast agents. Nonlinear excitation and frequency conversion microscopy imaging techniques do not require contrast agents but generally require complex instrumentation.[27] It has recently been demonstrated that AF microscopy under UV excitation provides visualization of cellular morphology and organization in *ex vivo* esophagus specimens without the use of contrast agents or tissue preparation.[28] Due to the

Table 1 Pretreatment biopsy classification and microscopically observed histologic abnormalities of the esophagus.

Pathology diagnosis	Histologic architecture	Cytology	Optical image morphology
BE no dysplasia	May have regular villous appearance of the surface epithelium.	Enterocytes and goblet cells.	Honeycomb-like pattern of columnar mucosa with goblet cells.
		Regular basal oriented nuclei without significant nuclear atypia	Goblet cells appear as round dark or bright features approximately 10 μm in diameter, with or without mucin content, respectively.
Indefinite for dysplasia	May have regular villous appearance of the surface epithelium.	Same as above, with nuclear atypia not extending to surface.	Polypoid-like projections similar to the gastric mucosa.
Low grade dysplasia	Same as above; minimal glandular irregularity.	Nuclear enlargement, high nuclear to cytoplasmic (N/C) ratio, hyperchromasia, pseudostratification extending to the surface.	Moderately disorganized tissue with loss of the specific cellular outline patterns characteristic of normal squamous or columnar epithelia.
		Goblet cell depletion.	Projections obscuring the flat surface of normal mucosa.
			Glandular crypts are visible as depressions or large, dark holes on the surface of columnar epithelium.
High-grade dysplasia	Irregularity and nodularity of the surface epithelium.	More severe hyperchromasia, pleomorphism, and nuclear membrane irregularity.	The mucosal surface is transformed into multiple papillary, villiform, or cauliform structures
	Irregular complex crypt architecture with back-to-back glands and cribiformation.	Prominent large nucleoli.	Surface becomes more three-dimensional, containing 3-D globular features.
		Loss of nuclear polarity.	Villi are recognized from visualization of their characteristic contour.
Malignant neoplasia	Additional highly irregular angulated glands, cords, nests, and single cells infiltrating into the lamina propria (intramucosal carcinoma) and through the muscularis mucosa into the submucosa (invasive adenocarcinoma).	Nuclear changes more severe than in HGD.	Highly disorganized tissue with loss of the specific cellular outline patterns characteristic of normal squamous or columnar epithelia.
	Prominent luminal necrosis.		Cauliflower-like projections 10 to 30 μm in diameter correspond to malignant features.
			Abnormal blood vascular patterns.

short propagation depth of UV excitation, the AF signal is confined in the epithelium, enabling acquisition of high-resolution images using high signal collection efficiency designs, such as widefield microscopy. This in turn allows clinically relevant cellular imaging using only the tissue's native fluorescence.

In this work, we present *ex vivo* results of AF microscopy under UV excitation from the esophagus, the stomach, and the intestine in order to establish optical patterns (rules of interpretation) that correspond to normal and abnormal histologies of the human esophagus and its transformation toward BE with subsequent dysplastic changes and progression to carcinoma. The results suggest that application of this method in a clinical setting could provide diagnostic information in real-time, which could be used by physicians as a tool to perform targeted biopsy/therapy and to obtain biopsy specimens that more accurately represent disease.

2 Materials and Methods

2.1 *Patient Enrollment and Tissue Sample Collection*

Eligible patients were identified and consented at the time of endoscopy by collaborating clinical investigators. The study protocol was approved by the University of California, Davis Medical Center (UCDMC) Institutional Review Board. Fifty-six patients undergoing routine surveillance endoscopy for Barrett's esophagus, dysplasia, and suspected esophageal cancer were enrolled in this clinical study. Four biopsy specimens were collected per patient for a total of 224 tissue samples. Biopsy specimens were collected with standard forceps and placed individually in labeled sterile containers with RPMI1640 media (Invitrogen, Carlsbad, CA). The first tissue biopsy specimen was taken from the proximal stomach (cardia). This was important in order to establish optical morphology of cardia mucosa as a control, as well as to rule out cardia adenocarcinoma.[7,12] The second control biopsy specimen was taken from the descending small intestine (duodenum). The third endoscopic biopsy specimen was taken from the distal esophagus and considered to be the pathological sample. The fourth biopsy specimen was taken from above the Z-line (squamocolumnar junction) in the squamous epithelium of the esophagus and was documented to be the normal esophageal control sample. Immediately after image processing, each biopsy specimen was placed in 10% formalin for fixation and transferred to pathology for tissue diagnosis. Each tissue biopsy specimen was taken to be histopathologically homogeneous such that the AF images were representative of the pathology diagnosis. The pathological evaluation was confirmed by at least two expert pathologists and taken as the diagnostic gold standard from which the optical images were categorized.

2.2 *Optical Imaging Protocol*

Each tissue sample was placed on a standard pathology cassette without preparation and with minimal handling. The tissue sample was covered with a quartz slide for imaging. This provided a flat imaging surface to keep the luminal plane of the small and irregularly shaped specimens in focus, which allowed for better visualization of cellular patterns. The quartz slide may not be necessary for future *in vivo* applications, as the tissue surface

may be better defined and aligned with the microscope's image plane.

The microscope imaging prototype platform has been previously described in detail.[29] In brief, a compact diode-pumped solid-state laser operating at 266 nm (Intelite, Minden, NV) was used as the photoexcitation source to generate the AF images. The *ex vivo* images under 266-nm excitation were acquired using a 5 second exposure time with an approximate dose of 30 mJ/cm^2 in order to optimize baseline image quality. The resulting AF images arose predominantly from the emission of tryptophan and provided a representation of the structure of the top layer of tissue cells. The microscope system was equipped with a 20× long working distance objective, followed by a 5× zoom lens. The images were recorded using a liquid nitrogen cooled charge-coupled device (Princeton Instruments, Trenton, NJ). The selected UV excitation wavelength propagated through the tissue to only about 50 μm, providing a sufficient amount of AF signal produced in the superficial tissue layer to be contained within the microscope's depth of field. This approach reduced the out-of-focus signal, allowing the formation of high-contrast images without optical sectioning techniques that reject most of the signal produced by the excitation light, that employ contrast agents, or that mandate time-intensive tissue preparation.[30] Our preliminary results indicated that microstructure morphology and superficial nuclear and cellular organization can be imaged in real-time, providing immediate information related to the presence and progress of early-stage abnormalities, such as BE and dysplasia, that originate in the superficial epithelial mucosa before developing into cancer.[28] Further development of this method necessitates the establishment of optical rules for recognizing cellular patterns (the rules for interpretation) that correspond to normal and abnormal histologies spanning from early benign modifications (Barrett's esophagus) to subsequent dysplastic change and progression toward carcinoma. Optical rules of disease interpretations that can be accepted by the medical community as an analogous guideline to traditional methods would provide the key to enabling *in vivo* histopathologic evaluation in the operating room.

2.3 *Approach for Developing Rules of Interpretation*

The images of the specimens in this study were compiled into a preliminary image gallery of normal and abnormal tissue structure that could be used to establish a correlation between image morphology and histopathology. We hypothesized that progression of abnormality was associated with the severity of deviation from normal structures observed in the UV AF images. Since BE required the presence of goblet cells, we included images of normal intestinal specimens in our study to establish the morphology of goblet cells (normally present in the intestine) to enable comparison with features observed in the images of BE. The intestine structure was also associated with the presence of villi and crypts, which were important recognition factors in the AF images. Furthermore, as the gastric type cellular morphology near the GE junction was shown to be associated with metaplastic progression, we included normal stomach tissue in this imaging study. Consequently, the analysis and categorization of the images for developing optical pattern recognition rules related to their histopathological state was focused on

distinguishing (a) normal esophageal tissue, (b) normal stomach and intestine tissue, (c) BE with no dysplasia, and (d) BE with dysplasia and cancer. Typical examples for each of these categories and results will be presented in separate subsections.

3 Results

3.1 Normal (Non-dysplastic) Esophageal Squamous and Columnar Epithelium Control Images

Figure 1 illustrates a squamocolumnar mucosal gold standard H&E section comparison with AF images of histologically unremarkable squamous [Fig. 1(a)] and columnar [Fig. 1(b)] tissue. Large, polygonal superficial cells that appear as individual tile-like structures with visible nuclei can be appreciated in both the H&E section and the normal esophageal squamous epithelium. It is notable that the optical images of nuclei were inconsistent in appearance. Decreased nuclear fluorescence has been described by Li et al.[31] in cultured cells but have also been observed in this work to display markedly increased signal intensity. Our previous work suggested that the discrepancy may be due to the maturation process of the stratified epithelia.[28] Many cells have no nuclei, while other nuclei can be small or undergoing pyknosis (densification). Imaging cells without nuclei, apoptotic cells, or pyknotic nuclei may produce variable optical signals that result in bright or dark features. These contrasting features may be attributed to the same microstructure, such as both bright and dark nuclei. A difference between the reduced intracellular columnar tissue intensity and increased cell membrane intensity can also be seen in Fig. 1(b). A typical microscopic UV AF image captured from specimens of normal columnar mucosa is shown. This image demonstrates visualization of the honeycomb pattern of cells showing their outlines with higher intensity compared with the cytoplasm region. We provided a quantitative assessment of this difference in a previous publication.[32] Our hypothesis that the origin of these images was due to the spectral contribution from different fluorophores including

tryptophan, NADH, flavoproteins, and/or lipopigments was supported by a calculated 30% intensity variation. The H&E staining of the non-dysplastic esophageal columnar mucosa section also demonstrates the typical honeycomb pattern observed in this type of tissue. These easily recognizable patterns observed in the UV AF images shown in Figs. 1(a) and 1(b) represent the characteristic morphology of the normal stratified squamous and columnar esophageal mucosa observed in fresh unprocessed specimens obtained without any tissue preparation. These typical examples of our observations were considered as the baseline (control) images for normal (healthy) esophageal tissue.

3.2 Normal Gastric and Intestinal Epithelium Control Images

The UV AF images shown in Figs. 2 and 3 represent typical examples of our results obtained from human biopsy specimens from normal duodenum (intestine) mucosa and normal cardia (proximal stomach) mucosa respectively. Due to the use of the quartz slide, the villi seen throughout this image appear as slightly compressed round structures. Figure 2 provides an artists' sketch from a luminal perspective (view of the endoscopist) showing villi apices, goblet cells, and columnar cells surrounding dark voids that represent crypts of Lieberkühn. It should be noted that crypts often represent imperfect glands that may be distorted, roundish, or otherwise inconsistent in appearance throughout the tissue surface. Furthermore, the crypt is a
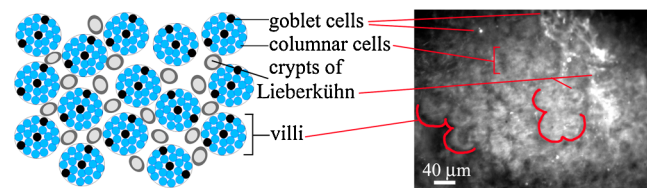
Fig. 2 Artist's sketch of normal duodenal microstructures from a luminal perspective (view of the endoscopist): villi apices, goblet cells, and columnar cells surrounding dark voids that represent crypts of Lieberkühn. These cartoon features (not drawn to scale) are indicated in the $475 \times 361\ \mu m$ field of view AF image of a duodenum tissue biopsy specimen. Villi apices are partially outlined for visual aid.
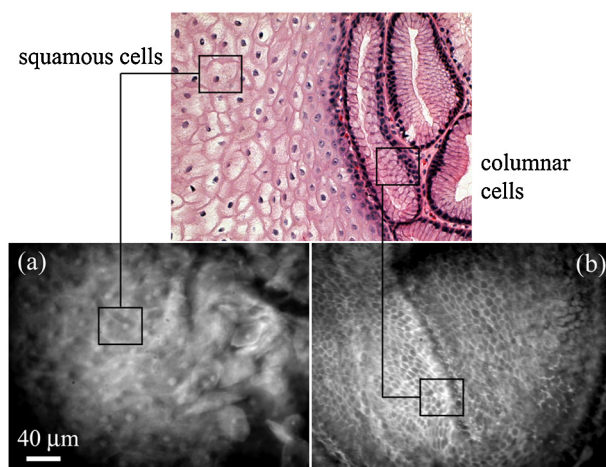
Fig. 1 Gold standard H&E squamocolumnar section compared with AF images of histologically unremarkable esophageal (a) squamous epithelial tissue with easily visible large polygonal superficial cells that appear as individual tile-like structures with nuclei that can be appreciated in both the H&E section and normal squamous epithelium, and (b) columnar epithelial tissue with the characteristic honeycomb pattern of cells showing their outlines with higher intensity compared with the cytoplasm region. Each field of view is $475 \times 361\ \mu m$.
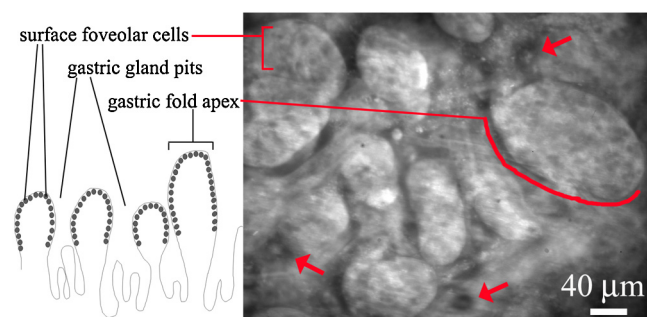
Fig. 3 Artist's sketch of normal cardia microstructures from a cross-sectioned perspective (view of the pathologist). The cartoon features (not drawn to scale) illustrate gastric fold projections with glandular pits at the mouth of the gastric neck and foveolar cells shown as dark, round features scattered throughout the surface. The corresponding $475 \times 361\ \mu m$ field of view AF image of a cardia tissue biopsy specimen is shown from a luminal view (view of the endoscopist). Arrows indicate what are believed to be gastric pits. A large gastric fold apex is partially outlined, with similar microstructures visible throughout the image.

depression around projecting villi and will not produce a detectable AF, thus appearing as dark features scattered throughout the luminal surface. Villi can also be deformed and distorted instead of resembling the ideal condition of pencil tips in a box. In the corresponding AF image of Fig. 2, the target-like features present as decreased signal voids, which may represent villi crypts similar to those observed in esophageal tissue previously reported.[32] Several examples are partially outlined for improved visualization. The dimpling and cramping of the uneven surface shown in the corresponding AF imaging are visible undulations of the duodenum epithelium with crypts and glands intervening between villi apices within the AF image of normal duodenal mucosa. The center apex had an approximate diameter of 40 to 50 μm. Similar rounded features were visible throughout the luminal surface. The heights of the villi typically varied from 0.5 to 1 mm, while their diameters varied from approximately one-eighth to one-third of their heights. Although the villi were compressed during imaging (to help better identify the goblet cells), their outlines are clearly visible within the image of Fig. 2, and their observed diameter is within the normal parameters. Based on the expertise of our collaborating pathologist, the duodenal tissue target-like feature of a dark area with one smaller dark spot and one inner brighter spot in Fig 2 was visibly similar in intensity contrast and diameter to an obvious esophageal tissue crypt of Lieberkühn. This crypt, detailed in Sec. 3.4 below in the cross-sectioned H&E image of Fig. 5, was identified during H&E microscopic evaluation as being from a duodenal location of biopsy. It is also visible in the corresponding AF image of Fig. 5. We hypothesize that the increased signal intensity is associated with higher tryptophan content or the presence of mucus-filled goblet cells, while darker features are associated with lower tryptophan concentration or the presence of a void.

As previously discussed, it is important to recognize and optically identify goblet cells in the AF images of the intestine. The nucleus of goblet cells is at their base, along with the organelles, while the remainder of the cell is filled with membrane-bound secretory granules filled with mucin. The "goblet cell" name comes from their cup-like shape. As goblet cells produce mucin, it was necessary to consider the different imaging results that mucin might produce if it is present inside the goblet cells of the fresh tissue biopsy specimens during AF imaging. Our experimental results strongly suggested that mucin typically produced an increased AF signal compared with the AF of the cells. Therefore, goblet cells containing mucin produced a much higher intensity than goblet cells without mucin within the fresh tissue, and served as an optical guideline documented in Table 1. These observations are illustrated with lines in the AF image of normal duodenum, shown in Fig. 2. A dark and a bright feature are indicated, each with a diameter of approximately 11 μm. We assumed that the dark feature is a goblet cell without mucin, while the bright feature is a goblet cell containing mucin. Similar features to those identified above could be found in the image shown in Fig. 2 and in similar images of normal intestine tissue. Thus, the results suggested that the goblet cells could be observed in the microscopic UV AF images as bright or dark features, on the order of 10 μm in diameter, depending on the mucin content at the time of imaging. Finally, two similar features that were believed to represent crypts of Lieberkühn of the duodenal epithelium are also indicated.

Figure 3 is an artists' sketch of cardia epithelium from a cross-sectioned perspective (view of the pathologist). The surface projections are gastric folds with glandular pits at the mouth of the gastric neck. Foveolar cells are shown as dark, round features scattered throughout the surface. The corresponding AF image of cardia mucosa in Fig. 3 is shown from a luminal perspective (view of the endoscopist) and was representative of such images obtained from normal stomach epithelium specimens. The gastric fold apices appear as large nodular features containing obvious dark outlines of foveolar cells scattered throughout the surface. Gastric pits, indicated with arrows, appeared as round target-like features similar to the duodenal crypts seen in Fig. 2. It should be noted that when correlating the AF images to the H&E gold standard, a 1:1 comparison of surfaces is inherently impossible. This is due to the tissue preparation of H&E sectioning, which results in an image of the foveolar cells below the neck (beyond penetration of AF image) due to removal of the luminal surface containing the gastric folds imaged in the AF technique. However, microscopic evaluation of the H&E images supported the observed tissue structures to correspond with those from the gastric biopsy location. The normal duodenum and cardia mucosal images such as those shown in Figs. 2 and 3 provided the control images to exemplify what microstructures of interest would look like using this imaging methodology. These AF images could be used as a baseline for comparison with images of specimens presenting benign intestinal metaplasia modifications of the esophagus, indicating BE, as discussed in the next section.

3.3 Visualization of Benign Epithelial Modifications

Figure 4 presents an esophagus biopsy specimen AF image that was collected at the endoscopically observed GE junction and returned with a pathological diagnosis of histologically unremarkable squamous esophageal mucosa with very scant columnar components. Cardia tissue topography characteristics are visible in the esophageal tissue, revealing gastric fold polypoid-like surface projections. Nobular rounded features may represent what could be irregular-surface mucous cells, squamous glands, or oxyntic metaplasia. The arrows point to larger, dark, target-like features that could be crypts similar to the duodenal and cardia crypts seen in Figs. 2 and 3. This
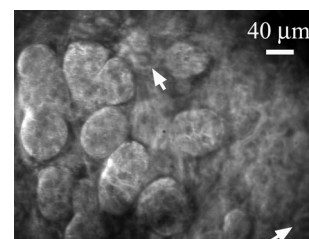

Fig. 4 475 × 361 μm AF image of an esophagus biopsy specimen that resembled the g1astric mucosa, as opposed to the squamous or columnar esophageal mucosa shown in Fig. 1. Arrows indicate dark, target-like features that could be crypts similar to the duodenal crypts seen in Fig. 2. Gastric fold polypoid-like surface projections are visible in the esophageal tissue, similar to those of the cardia tissue seen in Fig. 3. These nodular esophageal microstructures may represent what could be irregular surface mucous cells, squamous glands, or oxyntic metaplasia.

AF image of the distal esophagus clearly resembles the gastric mucosa of Fig. 3 as opposed to the squamous or columnar mucosa shown in Fig. 1. The scant honeycomb pattern was preserved in the columnar mucosa, similar to that shown in Fig. 1(b). The irregular polypoid surface appeared to be transitioning from squamocolumnar mucosa containing villi crypts (arrows), consistent with previous results.[28] The multiple projections might be seen as unfolding areas with glands, obscuring the flat surface of stratified squamous mucosa, and inhibiting a clear focus of features beneath the structures of greatest height. We commonly observed optical images of cardia-like esophageal mucosa as those seen in Fig. 4, which appear at first glance to be modified from the characteristic morphology of the nondysplastic or normal esophageal tissue shown in Fig. 1, but were not yet differentiated EAC (detailed in Sec. 3.6, Fig. 8 below. However, patient history must be considered when examining diagnostic results related to disease progression, especially for those on chronic medication. Many BE patients are placed on proton-pump inhibitors (PPIs) in an attempt to reduce associated acid reflux. PPI therapy is associated with several histological changes, including parietal cell and foveolar hyperplasia, as well as microcystic dilation of gastric glands. This transformation is a common observation in GE biopsies of the cardia mucosal cells. These surface nodularities, identifiable with UV autofluorescence microscopy, possibly correspond to the above-described PPI effect seen histologically and shown in Fig. 4. This could explain the commonly observed nodularity in the squamous esophageal mucosa in our study, which is reminiscent of fundic gland polyps generally seen in the gastric body in patients with BE on PPI therapy. Consequently, this UV AF method provides a clinically important distinction of normal gastric columnar mucosa that standard endoscopy is generally limited from distinguishing.

3.4 Visualization of Barrett's Esophagus and Early LGD

Figure 5 shows the H&E gold standard cross-sectioned image of an esophagus specimen from a patient with pathology diagnosis of BE with mild to moderate chronic inflammation and suspected LGD. This esophagus biopsy specimen was collected at 32 cm with an unlisted Z-line and GE junction. The
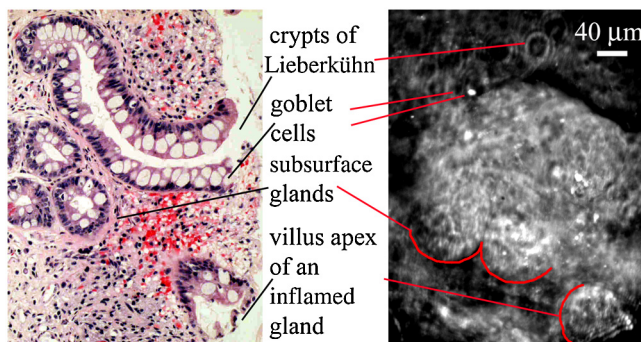

Fig. 5 The H&E gold standard 361×475 μm cross-sectioned view of human esophagus biopsy tissue with intestinal metaplasia (BE) features histopathologically determined crypts of Lieberkühn, goblet cells, subsurface glands, and villi apices. The luminal view of the accompanying AF image is of the same specimen with lines indicating what could be visibly correlated microstructures. A goblet cell without mucin (dark) and one with mucin (bright) are shown side by side.

corresponding UV AF image is of the same esophagus biopsy specimen. It should be considered for correlation purposes that features viewed from the surface with AF microscopy (endoscopist view) varied in diameter from H&E section (pathologist view of the biopsy specimen cross-section). The suspicion of LGD was histopathologically defined by the closely packed overlapping basal nuclei with hyperchromasia and irregular contours of H&E surface morphology, although the overall epithelial architecture appeared to be preserved, maintaining a degree of uniformity at the surface. Based on the criteria for the recognition in the AF images presented in the previous section, goblet cells, each with a diameter of approximately 10 to 15 μm, are shown in the AF image of this specimen. A goblet cell without mucin (dark), and with mucin (bright) are specified with lines and shown side by side. The indicated crypt of Lieberkühn was approximately 313 μm along the horizontal axis. A gland that had become inflamed and angulated resulting in visible architectural distortion is indicated at the lower right of the figure. Only the lower portion remains, resulting in an apparent triangular shape instead of the normal doughnut shape. This distorted and inflamed gland was approximately 104 μm in diameter with the villi apex beginning to project from the mucosa surface, possibly becoming further distorted during tissue biopsy removal. The cluster of four glands approximately 200 μm subsurface might attribute to the visible irregular contours at the surface. These microstructures can be seen from the luminal-plane AF image corresponding to the same indicator lines of the H&E image. Surface features in the UV AF image can be correlated with the 313 μm in diameter crypt of Lieberkühn gland. This feature had a target-like appearance with light and dark alternate rings and a diameter of approximately 30 to 35 μm. Similar features were observed throughout the same figure. Based on previous observations in various specimens, we hypothesize that the dark center represented the opening of a crypt toward the lumen of the gland,[32] shown in Fig. 2. The inconsistency of visibility could be attributed to the difference of height projection of villi into the luminal plane. Visible architectural distortion from both the AF epithelial surface as well as the H&E image may be due to the gland that had become inflamed and angulated.

The AF images shown in Fig. 6 were from two different patients and represented the images obtained from specimens with varying grades of BE. The biopsy specimen shown in Fig. 6(a) was collected at 39 cm (GE junction unlisted) and returned a pathology report of BE with reactive atypia. The biopsy specimen shown in Fig. 6(b) was collected at 32 cm, 1 cm above the Z-line (33 cm), with a GE junction located at 35 cm, and returned a pathology report of BE with moderate acute and chronic inflammation, indefinite for dysplasia. The optical features within the honeycomb structure (defined in Fig. 1), were previously assigned to represent villi, crypts, and goblet cells of the small intestine (see Fig. 2), and can be easily recognized with the progression to BE throughout the esophagus AF images shown in Fig. 6. For example, a large, dark feature that may represent villi apices is indicated with line 1 in Fig. 6(a). Villi may not be immediately apparent because a regular villous appearance was not always a characteristic of BE as it is of the duodenum. Line 1 in Fig. 6(b) indicates a feature that is consistently seen scattered throughout a honeycomb background. These features could be the formation of
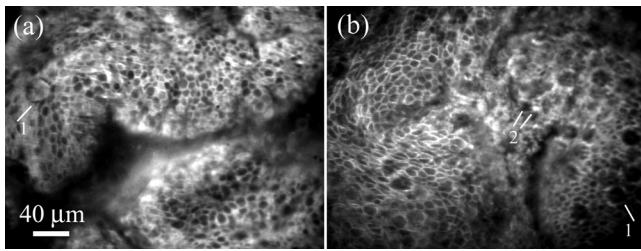
Fig. 6 475×361 μm field of view AF image of sections of human esophagus biopsies specimens of (a) BE with reactive atypia, and (b) BE with moderate acute and chronic inflammation, indefinite for dysplasia. Features indicated with lines are consistent with those identified in Fig. 2, possibly representing a villous apex [line 1, (a)], crypt of Lieberkühn [line 1, (b)], and goblet cells [line 2, (b)].

crypts of Lieberkühn as in Fig. 2. Dark and bright features were also visible and could be correlated to non-mucin and mucin filled goblet cells, indicated respectively with lines 2 in Fig. 6(b). The surface of the columnar mucosa retained a degree of normality and smoothness, an indication that dysplasia had not yet developed. The categorization of "indefinite for dysplasia" might not be visible from the surface epithelium, as this histologic abnormal progression was diagnosed using a traditional cross-section of tissue on a slide. Specific to these microstructures, it may be unlikely that the dark features, which are visible at higher density than those shown in Figs. 4 and 5 and identified as crypts, are nuclei, since the elongated nuclei of esophageal columnar epithelial cells are located toward the basal surface beyond the superficial imaging depth of this technique.[32] Rather, the increased frequency and density of features believed to be goblet cells and crypts of Lieberkühn may be attributed to disease progression as healthy squamocolumnar epithelium of the esophagus begins to transition toward intestinal metaplasia (Barrett's esophagus) that more closely resembles duodenal epithelium, shown in Fig. 2.

3.5 Low-Grade Dysplasia in BE

The esophagus AF images shown in Fig. 7 were from three different patients with a pathological diagnosis of LGD. The optical features of what are believed to represent villi, crypts, and goblet cells (defined in previous sections) could be recognized throughout Fig. 7. For example, the image of Fig. 7(a) has a very similar appearance to the BE images of Fig. 5. This biopsy specimen was collected from 34 cm just above the GE junction at 35 cm. The villi appear to maintain a degree of regularity as they are seen projecting from the surface epithelium. It is also possible that the rounded features are cardia-type
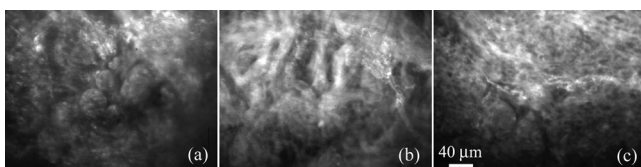
mucosa biopsied near the top of a hiatal hernia. There is a cloudy region in the upper right with bright streaks that might be a layer of mucous or vasculature appearing to overlay the luminal surface. The images of the tissue biopsy specimens shown in Figs. 7(b) and 7(c) have visible projections that obscure the flat surface of normal mature squamous epithelium, exemplified in Fig. 1. The overall surface pattern in the lower half of Fig. 7(b) appears to remain intact. The biopsy was collected from 36 cm. The snaking pattern in the upper half of Fig. 7(b) might represent the formation of pseudostratification extending to the surface, a cytology hallmark of LGD. The bright streaks across the center might indicate vascularization from injury or recovery from previous radiofrequency (RF) ablation therapy. Villi that appear to be forming in the lower half of Fig. 7(c) maintained a regular appearance more similar to those of the duodenum in Fig. 2. The Z-line was at 39 cm, and the GE junction was at 40 cm, the location of biopsy specimen collection. The image was increasingly out of focus as the surface became more three-dimensional, as opposed to the pavement-like surface of stratified squamous epithelium shown in Fig. 1.

3.6 High-Grade Dysplasia and Esophageal Adenocarcinoma

Figure 8 illustrates UV AF images of HGD and EAC. Each esophagus biopsy specimen shown in Fig. 8 was taken from a different patient. It can be easily appreciated that these images exhibit a high degree of deviation from the normal esophagus epithelium shown in Fig. 1. All of the images had an increasingly disorganized three-dimensional aspect, characteristic complex mucosal architecture, and villiform configuration that currently defines HGD and EAC. The image shown in Fig. 8(a) was obtained from a biopsy specimen with pathological diagnosis of squamocolumnar mucosa with HGD. The three-dimensional globular features visible on the mucosal surface cause a crowded villous topography and are reflective of HGD. Surface nodularity might also imply an early onset of carcinoma. Figs. 8(b) and 8(c) both demonstrated a more
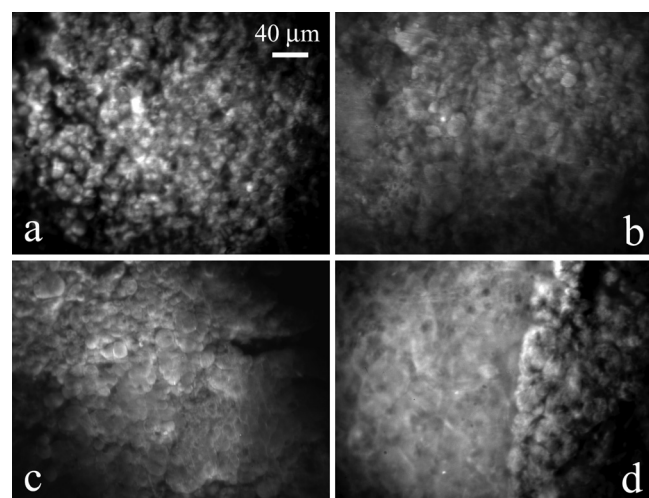

Fig. 7 475×361 μm field of view human esophagus biopsy specimens of (a) squamocolumnar mucosa with LGD, (b) BE with LGD, and (c) BE with LGD and visibly distorted surface architecture. Visible surface projections obscure the flat surface when compared with normal squamous and columnar epithelium, exemplified in Fig. 1.

Fig. 8 475×361 μm field of view AF images of human esophagus biopsy specimens obtained from different patients who were diagnosed with (a) HGD, (b) focal adenocarcinoma in a background of high- and low-grade dysplasia, (c) EAC, and (d) poorly differentiated EAC with obvious margin delineation between normal and diseased tissue.

cauliflower-like appearance than HGD, indicating EAC. Fig. 8(b) was obtained from a specimen with pathological diagnosis of focal adenocarcinoma in a background of high- and low-grade dysplasia. The villiform surface and disorganized mucosal pattern were easily differentiated from the stratified squamous epithelium of normal esophagus shown in Fig. 1. Mucosal crowding and disorganization were visible in the AF image and correlated with pathological assessment. Villiform features were visible as cauliflower-like projections, 10 to 30 μm in diameter, and corresponded to malignant features observed in the H&E section of this specimen. Features that correspond to crypts and goblet cells with a diameter of approximately 15 μm were also visible. Pathological diagnosis of EAC with similar image characteristics displaying an increasingly villiform surface and a disorganization of mucosal pattern can also be recognized in the images shown in Figs. 8(c) and 8(d). In Fig. 8(d), the pathological diagnosis was poorly differentiated adenocarcinoma. Margin delineation capability is exemplified, as the tissue on the left of the image resembled squamous mucosa shown in Fig. 1, while the tissue on the right of the image had more of a continuous mucosal and a cribriform growth pattern, similar to the pathologically diagnosed EAC shown in Fig. 8(c). There is a visible decrease of pattern regularity with progression of disease observed as tissue transitions from HGD [see Fig. 8(a)] to EAC [see Figs. 8(b)–8(d)]. Additionally, EAC was characterized by the proliferation of small, irregular glands that contributed to the overall cauliflower-like appearance that was especially visible in Figs. 8(b) and 8(c). Currently it is extremely difficult to differentiate HGD and EAC,[12] and a histologic criterion that defines a diagnosis of intramucosal cancer has not yet been published.[13] Figure 9 provides an optical histological progression of esophageal morphology, from normal squamous to invasive carcinoma. The epithelial distortion is obvious even to the untrained eye. A preliminary set of optical rules for interpretation is tabulated in the "Optical Image Morphology" column of Table 1.

4 Discussion

Recent work has shown that the gastroesophageal (GE) junction harbors the first stages of intestinal metaplasia.[9,11] Arguably, providing an imaging technology that identifies goblet cells *in vivo* (such as the technique presented in this work) would allow for early detection of intestinal metaplasia within columnar (non-squamous) mucosa of the distal esophagus. Identification of goblet cells becomes less meaningful when dysplasia or cancer is detected. Technology that can identify microscopic dysplastic changes would enable biopsy specimens to be
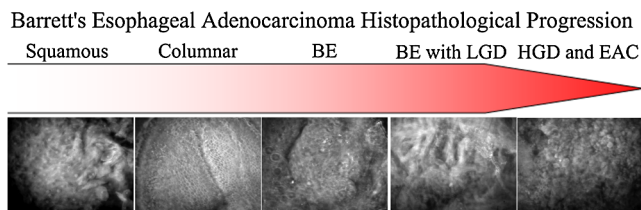
Barrett's Esophageal Adenocarcinoma Histopathological Progression

| Squamous | Columnar | BE | BE with LGD | HGD and EAC |

Fig. 9 Visible progression of premalignancy changes in Barrett's esophageal adenocarcinoma, starting from normal squamous mucosa (far left) to invasive carcinoma (far right), discussed in detail in Figs. 1, 5, 7, and 8.

collected in suspiciously abnormal regions, compared with current practice of random biopsy. This is particularly important in long-segment BE, which currently necessitates time-consuming multiple biopsies to ensure adequate sampling.

The imaging approach presented in this work provides visualization of morphological changes of the epithelial layer, where 85% of all cancers initiate.[33] Several hardware variations have been previously described[28,30] to mitigate mutagenic concerns arising from UV dosage to wavelengths between 180 and 302 nm, and to achieve the defined 3 mJ/cm^2 *in vivo* maximum permissible exposure (MPE).[34] In brief, the current microscope configuration does not transmit UV light, the spectral range containing a predominant amount of tryptophan emission. Second, the CCD detector used for image acquisition had just 30% quantum efficiency (QE) between 400 and 450 nm, where most of the detected signal was concentrated. Third, decreasing the acquisition time to less than 1 s would decrease the UV exposure level without significant deterioration to the overall visual perception of image quality. Consequently, these three improvements could optimize signal-detection efficiency and lead to a reduction in exposure dosage below the ANSI-defined MPE of 3 mJ/cm^2 while providing real-time diagnostic images for future *in vivo* application. The goal of this preliminary *ex vivo* work was to explore the potential of this method to provide real-time histological information that does not rely on contrast agents or other types of tissue preparation. We postulate that this approach may have associated savings in cost and time, which are especially critical during an upper endoscopy when the duration of the procedure can be very short. The UV AF images of mucosal biopsy specimens presented in this work are evaluated based on their pretreatment classification, which is the gold standard of BE diagnosis.[21] The results of our study suggest that this method may have a high degree of impact diagnosing LGD and HGD, the endpoints of dysplastic staging where pathology has yet to be defined. Histopathologic criteria for LGD and HGD have been proposed and documented in numerous publications and textbooks in the medical literature, yet the differentiation between LGD and HGD associated with BE has been a source of diagnostic discrepancy even among specialized expert GI pathologists, associated with low inter- and intraobserver reproducibility. Quantification of optically visible observations may provide the fingerprint for defining the endpoints of dysplasia by simultaneously providing targeted biopsy to the endoscopist and reducing interobserver variability. Therefore, interpretation of the images provided with this method can be achieved using the classical knowledge of disease progression without a need to develop an entirely new set of approaches for the interpretation of the images. Based on our findings, we have developed a preliminary set of rules for interpreting the UV AF images that are summarized in column 4 of Table 1, "Optical Image Morphology." In general, all examined specimens followed the optical rules outlined in Table 1 and are shown as a visible progression of AF microscopy images in Fig. 9. This set of optical rules will provide future studies with the baseline from which statistical evaluation could be attempted. Based on a set of quantified statistical results, the optical rules may be further enhanced or modified. Once this stage has been reached, future work could be considered to implement statistical approaches to determine the diagnostic accuracy (sensitivity and specificity) using

standard pathology as a reference. This approach could employ powerful algorithms, such as parallel factor analysis (PARAFAC) conducted for the first time on biological tissues to differentiate carcinoma from normal nasopharyngeal tissue.[35]

Analogous to the confocal Barrett's classification, Table 1 serves as a foundation from which to build on.[25,26] As it has taken decades to correlate abstract images of stained tissue sections and establish traditional histology, a similar effort may be needed to establish the correlation of characteristic features observed in the images obtained using new technologies such as the UV AF microscopy method discussed in this work. It must be noted that this method is insensitive when disease characteristics lack appearance or alteration of epithelial features. One such example is the case of "indefinite for dysplasia," which lacks changes in the surface epithelium, making evaluation of surface maturation difficult.[21] Mucosal features are a critical guideline for both optical imaging and the pathologist's evaluation of the presence or absence of surface maturation, an important feature that helps to determine regeneration versus dysplastic changes.[21]

From 1998 to 2005, esophageal disorder related hospitalizations increased by 216%, with associated costs increasing by 289%.[36] It has been acknowledged that the current tradition of collecting random biopsy specimens and classifying these samples using a method fraught with variability reduces the likelihood of finding a treatable neoplasia to chance.[7] 30% of endoscopic resection cases have recurrent neoplasia due to missed segments of disease during endoscopy, and 40% to 60% of patients may already have an invasive malignancy by the time a biopsy specimen accurately reveals high-grade dysplasia to the pathologist.[37,38] A reduction of biopsied tissue for preparation and reading would save drastically in both cost and time, as well as improve patient quality of life. Thus, an endoscopic imaging system that provides real-time histology of early esophageal disease without the additional cost of contrast agents or preparation time has a potential cost saving comparable to breast cancer screening (mammography) and cervical cancer screening (Pap smear).[39] The change of traditional methods comes with the challenge of implementing and interpreting histology-like optical images. The adaptation of new technology will depend on producing highly reproducible, specific, and sensitive information that correlates with the familiar and established guidelines of disease diagnosis.

Acknowledgments

References

1. N. J. Shaheen and J. E. Richter, "Barrett's oesophagus," *Lancet* **373**(9666), 850–861 (2009).
2. P. Enzinger and R. Mayer, "Esophageal cancer," *N. Engl. J. Med* **349**(23), 2241–2252 (2003). http://www.nejm.org/doi/full/10.1056/NEJMra035010
3. I. Qureshi, M. Shende, and J. Luketich, "Surgical palliation for Barrett's esophagus cancer," *Surg. Oncol. Clin. N. Am* **18**(3), 547–560 (2009).
4. M. Pera et al., "Epidemiology of esophageal adenocarcinoma," *J. Surg. Oncol.* **92**(3), pp. 151–159 (2005).
5. H. Pohl and H. Welch, "The role of overdiagnosis and reclassification in the marked increase of esophageal adenocarcinoma incidence," *JNCI Cancer Spectrum* **97**(2), 142 (2005).
6. N. Shaheen and D. Ransohoff, "Gastroesophageal reflux, Barrett esophagus, and esophageal cancer: scientific review," *JAMA* **287**(15), 1972 (2002).
7. K. J. Lewin, R. H. Riddell, and W. M. Weinstein, *Gastrointestinal Pathology and Its Clinical Implications*, IGAKU-SHOIN Medical Publishers, Inc., New York ISBN 0896401537 (1992).
8. S. Spechler et al., "Prevalence of metaplasia at the gastro-oesophageal junction," *The Lancet* **344**(8936), 1533–1536 (1994).
9. J. H. Peters, T. J. Watson, and T. R. DeMeester, "Esophageal anatomy and physiology and gastroesophageal reflux disease," in *Greenfield"s Surgery: Scientific Principles and Practice*, pp. 674–677, Lippincott Williams and Wilkins, Philadelphia, PA (2006).
10. J. Lenglinger et al., "Barrett's esophagus: size of the problem and diagnostic value of a novel histopathology classification," *Eur. Sur.* **41**(1), 26–39 (2009).
11. J. Lenglinger et al., "Update: histopathology-based definition of gastroesophageal reflux disease and Barrett's esophagus," *Eur. Sur.* **40**(4), 165–175 (2008).
12. T. W. Rice, J. E. Mendelin, and J. R. Goldblum, "Barrett's esophagus: pathologic considerations and implications for treatment," *Semin. Thorac. Cardiovasc. Surg.* **17**(4), 292–300 (2005).
13. E. Downs-Kelly et al., "Poor interobserver agreement in the distinction of high-grade dysplasia and adenocarcinoma in pretreatment Barrett's esophagus biopsies," *Am. J. Gastroenterol.* **103**(9), 2333–2340 (2008).
14. G. Y. Lauwers et al., "Novel endoscopic therapeutic modalities for superficial neoplasms arising in Barrett's esophagus: a primer for surgical pathologists," *Mod. Pathol.* **22**(4), 489–498 (2009).
15. H. Mork et al., "High recurrence rate of Barrett's epithelium during long-term follow-up after argon plasma coagulation," *Scand. J. Gastroenterol.* **42**(1), 23–27 (2007).
16. S. Wani et al., "Esophageal adenocarcinoma in Barrett's esophagus after endoscopic ablative therapy: a meta-analysis and systematic review," *Am. J. Gastroenterol.* **104**(2), 502–513 (2009).
17. M. I. Canto et al., "Low flow CO_2-cryotherapy for high risk Barrett's esophagus (BE) patients with high grade dysplasia and early adenocarcinoma: a pilot trial of feasibility and safety," *Gastrointest. Endosc.* **67**(5), Ab179–Ab180 (2008).
18. S. R. DeMeester, "New options for the therapy of Barrett's high-grade dysplasia and intramucosal adenocarcinoma: endoscopic mucosal resection and ablation versus vagal-sparing esophagectomy," *Ann. Thorac. Surg.* **85**(2), S747–S750 (2008).
19. V. Sharma et al., "Balloon-based, circumferential, endoscopic radiofrequency ablation of Barrett's esophagus: 1-year follow-up of 100 patients," *Gastrointest. Endosc.* **65**(2), 185–195 (2007).
20. M. Stolte, "The new Vienna classification of epithelial neoplasia of the gastrointestinal tract: advantages and disadvantages," *Virchows Arch.* **442**(2), 99–106 (2003).
21. R. D. Odze, "Diagnosis and grading of dysplasia in Barrett's oesophagus," *J. Clin. Pathol.* **59**(10), 1029–1038 (2006).
22. G. W. Falk, "Risk factors for esophageal cancer development," *Surg. Oncol. Clin. N. Am.* **18**(3), 469–485 (2009).
23. M. Wallace and P. Fockens, "Probe-based confocal laser endomicroscopy," *Gastroenterology* **136**(5), 1509–1513 (2009).
24. M. Nakao et al., "Optical biopsy of early gastroesophageal cancer by catheter-based reflectance-type laser-scanning confocal microscopy," *J. Biomed. Opt.* **13**(5), 054043 (2008).
25. R. Kiesslich et al., "In vivo histology of Barrett's esophagus and associated neoplasia by confocal laser endomicroscopy," *Clin. Gastroenterol. Hepatol.* **4**(8), 979–987 (2006).
26. K. Dunbar et al., "Confocal laser endomicroscopy in Barrett's esophagus and endoscopically inapparent Barrett's neoplasia: a prospective, randomized, double-blind, controlled, crossover trial," *Gastrointest. Endosc.* **70**(4), 645–654(2009).

27. D. Li, W. Zheng, and J. Qu, "Imaging of epithelial tissue in vivo based on excitation of multiple endogenous nonlinear optical signals," *Opt. Lett.* **34**(18), 2853–2855 (2009).

28. B. Lin et al., "Real-time microscopic imaging of esophageal epithelial disease with autofluorescence under ultraviolet excitation," *Opt. Exp.* **17**(15), 12502–12509 (2009).

29. S. G. Demos et al., "Imaging of tissue microstructures using a multi-modal microscope design," *IEEE J. Sel. Top. Quant.* **11**(4), 752–758 (2005).

30. B. Lin et al., "Endomicroscopy imaging of epithelial structures using tissue autofluorescence," *J. Biomed. Opt.* **16**(4), 046014 (2011).

31. D. Li, W. Zheng, and J. Y. Qu, "Two-photon autofluorescence micros-copy of multicolor excitation," *Opt. Lett.* **34**(2), 202–204 (2009).

32. B. Lin et al., "Characterizing the origin of autofluorescence in human esophageal epithelium under ultraviolet excitation," *Opt. Exp.* **18**(20), 21074–21082 (2010).

33. J. W. Tunnell et al., "Instrumentation for multi-modal spectroscopic diagnosis of epithelial dysplasia," *Technol. Cancer Res. Treat.* **2**(6), 505–514 (2003).PMID: 14640762

34. A. N. S. Institute, "American National Standards Institute for Safe Use of Lasers, Z136.1-2000" (2000) http://www.ansi.org.

35. B. Lin et al., "Diagnosis of early stage nasopharyngeal carcinoma using ultraviolet autofluorescence excitation–emission matrix spectro-scopy and parallel factor analysis," *Analyst* **136**(19), 3896–3903 (2011).

36. Y. Zhao et al.HCUP, "Healthcare Cost and Utilization Project," (2008). http://www.ahrq.gov/data/hcup; http://www.hcup-us.ahrg.gov/reports/statbriefs/sb44.pdf

37. M. J. Schuchert and J. D. Luketich, "Barrett's esophagus—emerging concepts and controversies," *J. Surg. Oncol.* **95**(3), 185–189 (2007).

38. F. P. Peters et al., "Stepwise radical endoscopic resection is effective for complete removal of Barrett's esophagus with early neoplasia: a prospective study," *Am. J. Gastroenterol.* **101**(7), 1449–1457 (2006).

39. M. J. Schuchert, K. McGrath, and P. O. Buenaventura, "Barrett's eso-phagus: diagnostic approaches and surveillance," *Thorac. Cardiovasc. Surg.* **17**, 301–312 (2005).